Desalination and Water Treatment
www.deswater.com

doi: 10.5004/dwt.2023.30148

315 (2023) 364–372
December

Resource and stabilization cotreatment of metallurgical arsenic-alkali slag and siderite via scorodite formation

Xinrong Su[a], Rui Su[a], Yanjiao Gao[a], Yinwen Bai[a], Xuanyu Li[a], Baochuan Qi[b,*]

[a]*College of Civil Engineering and Architecture, Liaoning University of Technology, Jinzhou 121001, China, emails: 220586004@stu.lnut.edu.cn (X. Su), surui@lnut.edu.cn (R. Su), tmgyj@lnut.edu.cn (Y. Gao), 2334210887@qq.com (Y. Bai), 3349212275@qq.com (X. Li)*

[b]*Key Laboratory of Pollutant Chemistry and Environmental Treatment, College of Resources & Environment, Yili Normal University, Yining 835000, China, Tel.: +86 0999 8137647; Fax: +86 0999 8137647; email: baochuanqi@yeah.net*

Received 14 August 2023; Accepted 20 November 2023

ABSTRACT

Arsenic-alkali slag (AAS) is one of the most hazardous solid wastes generated by the antimony smelting process, posing a significant environmental risk. However, the economic method for effective As immobilization in AAS is still lacking. In this study, we proposed an economical and novel method for the removal of As from AAS using siderite ($FeCO_3$). After the sodium carbonate is recovered from the AAS leaching liquor, the process continues. Aqueous As(V) is immobilized as scorodite via continuous dissolution–oxidation of siderite ($FeCO_3$) by air injection. The residual As(V) is immobilized via Fe-As coprecipitation by lime neutralization. The dissolution–oxidation of siderite produces Fe(III), ensuring continuous Fe(III)-As(V) coprecipitation and scorodite crystallization. The results showed that the removal efficiency of As from AAS reached 99.98%. The mixture of scorodite and Fe-As coprecipitation demonstrated good As stability in the Toxicity Characteristic Leaching Procedure (2.6 mg/L) and at pH 4 (1.84 mg/L), pH 6 (2.13 mg/L), and pH 8 (3.20 mg/L) in a 50-d long-term stability test. Combined results from chemical analysis, X-ray diffraction, and infrared spectroscopy revealed that the existence of high ionic strength Na^+ and Cl^- were the critical factors in the dissolution of siderite and the crystallization of scorodite. This study provides an effective treatment method for the removal and fixation of arsenic in metallurgical AAS.

Keywords: Arsenic-alkali slag; Siderite; Scorodite; Fe-As coprecipitation

1. Introduction

Arsenic-alkali slag is known as the most hazardous byproduct of the antimony (Sb) smelting industry [1]. China possesses 56% of the world's antimony reserves, the most abundant Sb resource globally. Currently, the amount of historically generated arsenic-alkali slag (AAS) has reached 2×10^5 tons in the Xikuangshan area, China, with an average annual yield of 5~6 × 10^3 tons [2–4]. Arsenic-alkali residue mainly contains Na_2CO_3 with a considerable amount of soluble $Na_2HAsO_4{\cdot}7H_2O$ and $NaSb(OH)_6$ [5,6]. Direct discharge of AAS into the environment poses a serious threat to human health and ecosystems [7,8]. Hence, As in AAS must be immobilized as stable solids for safe disposal.

Currently, various treatment methods have been developed, including *in-situ* stabilization, cement solidification/stabilization (S/S), As(V) reduction with SO_2 treatment, and resource recovery followed by As fixation. The *in-situ* stabilization method is based on the idea that the *in-situ* addition of curing agent, such as Fe(II) or Fe-(hydr)oxides into AAS could transform the soluble $Na_2HAsO_4{\cdot}7H_2O$ and Sb-containing compounds into insoluble Fe-As and Fe-Sb

* Corresponding author.

bearing precipitates (arsenical and antimonyal Fe-(hydr) oxides) [9,10]. Cement solidification/stabilization is based on the idea that an inert material and a binder are used to prevent physical contact between the AAS and the surrounding environment [11]. However, these two methods would significantly increase the bulk volume of the residue because of the high demand for curing agents and inert materials. Furthermore, the Sb and Na_2CO_3 resources that existed in AAS could not be recycled. The As(V) reduction with SO_2 and evaporation concentration to recover arsenic is proposed to dispose of the AAS, but the recovered As_2O_3 is easy to introduce secondary high-toxicity pollutants [7,12,13]. In contrast, resource recovery followed by As fixation is an attractive treatment method for AAS. This treatment method via water leaching could effectively separate As and Na_2CO_3 from insoluble Sb-bearing precipitate [14–16] and recover Na_2CO_3 via injection of CO_2 or evaporation crystallization [4,6,12,17]. Lime neutralization–precipitation or iron-arsenic coprecipitation methods are commonly used to remove and fix As in the residual liquid [4,18–21]. However, the lime neutralization precipitation method could produce a huge amount of hazardous arsenic-calcium residue with poor water stability [22–25]. While the iron-arsenic coprecipitation method can generate the stable Fe-As residue in AAS treatment, but the demand for Fe reagent is high [6,26]. Hence, the majority of AAS has not yet been adequately handled due to a lack of suitable treatment methods.

Scorodite ($FeAsO_4{\cdot}2H_2O$) is an attractive As-carrier because of its high As content (As ~32 wt.%), high Toxicity Characteristic Leaching Procedure (TCLP) stability, and low demand for Fe (Fe/As = 1) [27–32]. Based on the concept that the well-crystalline scorodite can form via control of the supersaturation degree of aqueous ferric arsenate by slow dissolution of natural iron minerals, economic Fe sources, such as natural iron minerals, have been applied to As removal and immobilization in waste sulfuric acid via scorodite formation [33,34]. Utilizing inexpensive Fe sources can significantly reduce the operation costs in fixing As in waste sulfuric acid and treating As-bearing solutions (Table 1). Su et al. [35] found that the utilization of natural siderite ($FeCO_3$) as a Fe source showed great advantages for the removal and fixation of As in waste sulfuric acid via scorodite formation. Under the optimal process condition ($pH_{initial}$ 1.1, Fe/As ratio 2, temperature 95°C, and reaction time = 10 h), the removal efficiency of As reaches 99.9% with a residual As concentration of 0.81 mg/L, and high TCLP stability of solid product (As <0.2 mg/L). Simultaneously, the deep As scavenging could be realized via Fe-As coprecipitation method because of the residual Fe in the filtrate after scorodite formation. Hence, we extrapolated that siderite could be used as the cheapest Fe(III) source for the fixation of As in AAS.

Table 1
Price of the common Fe source [36]

Fe source	$FeCO_3$	$FeSO_4{\cdot}7H_2O$	$Fe_2(SO_4)_3$	$FeCl_3{\cdot}6H_2O$
Price (USD/ton·Fe)	246	363	586	2,163

In this study, we proposed an alternative method for resourceful treatment and deep arsenic removal from AAS via scorodite, followed by Fe-As coprecipitation, using natural siderite ($FeCO_3$) as an iron source. The method not only avoided the environmental pollution from AAS, but also the treatment cost was greatly reduced due to low prices for siderite.

2. Materials and methods

2.1. Materials

The arsenic-alkali slag (AAS) was directly collected from an Sb refinery in the Xikuangshan mining area, China. Siderite ($FeCO_3$), purchased from Maya Reagent Company Ltd., (Zhejiang, China), was utilized as an iron source for scorodite formation. All experiments were conducted with industrial-grade reagents, tap water, and 5% HNO_3 cleaned glassware.

2.2. Experimental methodology

2.2.1. As solution preparation

Water leaching was conducted to separate soluble arsenate and carbonate from insoluble Sb-bearing minerals. The carbonate was recovered as sodium bicarbonate ($NaHCO_3$) via the injection of air (21% CO_2) and then solid/liquid separation (Fig. S1). The obtained alkaline As-enriched solutions were acidized to pH 0.4 and 1.1 (denoted as AAS-0.4 and AAS-1.1) by adding HCl with the systems stirred vigorously (300 rpm). The NaOH-neutralized As_2O_5 solution with pH 1.1 (denoted as FAO-1.1) and As concentration equivalent to AAS-1.1 was applied to compare the effect of excessive Na^+ ions on As immobilization.

2.2.2. Preliminary As fixation via scorodite formation

The above-mentioned As-enriched solution was heated to 95°C with slowly stirring (200 rpm). An amount of siderite powders, that is, Fe/As = 2, was added to the As-enriched solution. Then the slurry was further stirred for 10 h and accompanied with the air injection at a flow rate of 0.1 L/min. Aliquots of suspension were collected at pre-designed time intervals (i.e., 2, 4, 6, 8, 10 h). The solids and liquids were then separated using 0.22 μm membranes. The supernatants were analyzed for the concentrations of As and Fe. The solids were washed three times using diluted HCl solutions with the same pH as the reaction system, then vacuum-dried at 40°C for 24 h. The suspension from the AAS-0.4 system after reaction for 10 h was retained for deep As removal.

2.2.3. Deep As removal via Fe-As coprecipitation

The slaked lime (2 mol/L $Ca(OH)_2$) was slowly added to the above-mentioned suspension from the AAS-0.4 system at room temperature (22°C), and agitated at a rate of 300 rpm with an agitator. Different initial pH values (4, 5, and 6) were tested to synthesize Fe-As precipitation and find the optimal reaction conditions. During the reaction, the pH values of the slurry were maintained using 0.01/0.1 mol/L $Ca(OH)_2$ and/or HCl solutions. The supernatants were separated by pressure filtration through a 0.22 μm membrane. The solids

from the pH 6 system were washed three times using diluted HCl solutions with the same pH as the reaction system, then vacuum-dried at 40°C for 24 h.

2.3. Analytical methodology

2.3.1. Elemental analysis

The concentrations of As were determined using an atomic fluorescence spectrometer linked with a hydride generator (AFS, Haiguang, China). The detection limit for As was 0.01 μg/L with an uncertainty of ±5%. The concentrations of Fe were determined using a flame atomic absorption spectroscopy (FAAS, Varian, USA). The content of CO_3^{2-} in the AAS was analyzed by chemical analyses [37]. The other elements were analyzed in AAS using X-ray fluorescence spectrometer (Priums, Japan).

2.3.2. Solid characterization

A Rigaku D/Max 2400 X-ray diffractometer (Rigaku, Tokyo, Japan) equipped with a cobalt target (Co $K\alpha_1$ radiation, λ = 1.7902), which was run at 56 kV and 182 mA, was used to describe the mineralogy of the solid products. All the X-ray diffraction (XRD) patterns of samples were scanned from 10° to 80° 2θ with increments of 0.04° 2θ. The infrared spectra of the solid samples were measured in the mid-infrared range (600–4,000 cm^{-1}) using a Fourier-transform infrared (FTIR) spectrometer (Nicolet 6700, Thermo Fisher Scientific, USA) in transmission mode. Before measurements, approximately 5 mg of finely ground powders mixed with 200 mg of high-purity KBr were pressed into a disk. Each sample was scanned 128 times, and averaged data were reported. The crystal morphology and elemental compositions of the solid samples were characterized using a scanning electron microscope combined with an energy-dispersive X-ray spectrometer (SEM-EDX, ProX, Phenom, Holland).

2.3.3. Stability analyses

TCLP was used to evaluate the short-term stability of final products. In brief, 1 g of products was placed in 20 mL of an acetic acid-sodium acetate mixed buffer solution (pH 4.93 ± 0.05) leached for 18 h agitation of 50 rpm, and a temperature of 22°C. The As leaching concentration is regulated at 5.0 mg/L, according to the hazardous solid waste identification guidelines.

The long-term stability tests were performed under atmospheric conditions for 50 d by adding 1 g of solid samples to 100 mL of HCl/NaOH solution at pH values of 4, 6 and 8. During the test, the pH of the suspensions was maintained constant with HCl or NaOH solutions.

3. Results and discussion

3.1. Characteristics of AAS and siderite

The bulk chemical composition reveals that AAS contains 3.7 wt.% As, 1.4 wt.% Sb, 23 wt.% Na, and 31 wt.% CO_3^{2-}, along with trace amount of Fe (Table 2), which is consistent with the SEM-EDX results (Fig. 1a). The XRD patterns indicated that the dominant crystalline phase in AAS are $Na_3H(CO_3)_2{\cdot}2H_2O$ and $NaSb(OH)_6$. No crystalline phase of As is identified by XRD in the AAS, suggesting As occurs as amorphous form, in agreement with the literature [9]. The mineralogical characteristic of siderite has been confirmed by XRD (Fig. 1b).

Table 2
Composition of the initial arsenic-alkali slag

Element	As	Sb	Na	CO_3^{2-}	Fe
wt.%	3.7	1.4	23	31	1.2

3.2. Preliminary As removal via scorodite formation

3.2.1. Composition evolution of the liquid phase

The effect of the initial pH value on the kinetic changes of dissolved As and Fe concentrations in different systems is investigated (Fig. 2a). In general, the concentrations of As and Fe decreased with increasing reaction time in all experiments (Fig. 2a and b). For the FAO-1.1 system, the concentration of dissolved As decreased from 88 to 3.2 mmol/L after reaction for 10 h, which corresponded to a final As removal efficiency of 96.3%. The concentration of Fe decreased from 176 to 15.4 mmol/L, resulting in a final Fe/As ratio of 4.8. The liquid composition evolution of the AAS-1.1 is different from that of FAO-1.1. The concentration of As decreased from 88 to 44.9 mmol/L with a low As removal efficiency of 48.9% and low Fe residual concentration of 4.5 mmol/L after the AAS-1.1 system reaction for 10 h. This difference might be attributed to the higher concentrations of Na^+ and Cl^- in the AAS-1.1 system compared to the FAO-1.1 system. The existing Na^+ and Cl^+ do not interfere with the secondary mineral phase formed in our studied systems [38]. However, the high ionic strength, due to the presence of Na^+ and Cl^+ ions, might alter the water structure and hydration of mineral surfaces, potentially inhibiting siderite dissolution and the crystallization of secondary minerals necessary for As immobilization in the AAS-1.1 system [39].

The initial pH value played a key role in affecting the dissolution of siderite and the release of Fe ions [39]. In this study, the lower pH values corresponding to relatively high H^+ concentrations were applied to dissolve the siderite to provide the Fe ions for Fe-As phase formation. With the increase in reaction time, the concentration of dissolved Fe decreased gradually in the AAS-0.4 system. The concentration of Fe reached the maximum of 100 mmol/L after reaction for 2 h. Notably, the dissolved Fe concentration was almost maintained at a constant of ~88.2 mmol/L after reaction for 6 h. The removal efficiency of As maintained a constant at ~ 67.4% after 6 h. In comparison to the AAS-1.1 system, the removal efficiency of As only increased from 48.9% to 67.4%, whereas the concentration of Fe increased from 4.5 to 88.2 mmol/L. These results suggest that a lower pH value can significantly increase the solubility of siderite. However, at low pH, the solubility of scorodite will be decreased, which affects the removal efficiency of As. It has been suggested that a pH range of 1–1.2 favors the transformation of amorphous ferric arsenate to scorodite [40]. The decreased initial pH does not substantially improve the removal efficiency

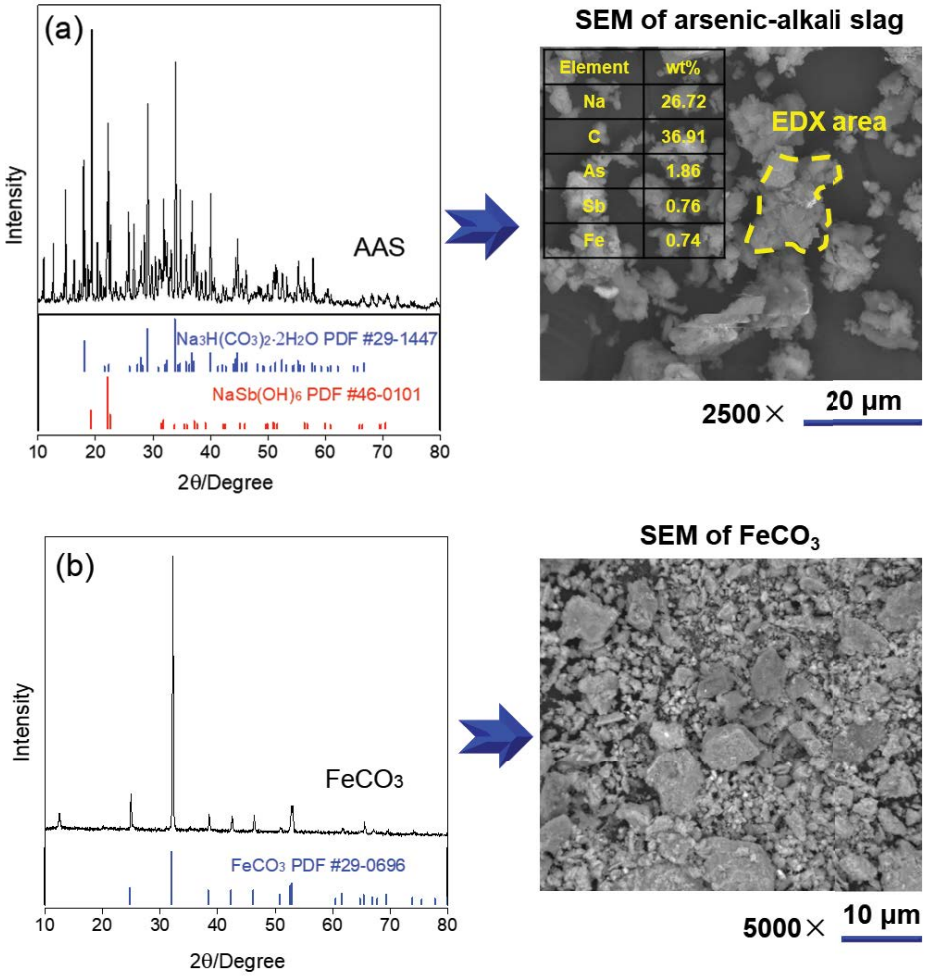

Fig. 1. X-ray diffraction patterns and SEM-EDX images of (a) initial arsenic-alkali slag and (b) siderite. The vertical bars represent the standard X-ray diffraction patterns of $Na_3H(CO_3)_2{\cdot}2H_2O$ (PDF #29-1447) and $NaSb(OH)_6$ (PDF #46-0101), and $FeCO_3$ (PDF #29-0609).

of As, but the Fe/As molar increased from 0.1 to 3.1 in the liquid phase, which provides a Fe-enriched source for subsequent fixation of As by lime neutralization to form Fe-As precipitation.

3.2.2. Solid-phase analysis

To study the mineralogy and surface chemical properties evolution of the transformation products, the solid samples generated at different reaction times in various systems are characterized using XRD and FTIR spectroscopy (Fig. 3). The mineral phases in solid products were highly dependent on the reaction system. XRD results suggested that scorodite was the dominant crystalline phase in the transformation products after reaction for 2 h in the FAO-1.1 system, implying the fast dissolution rate of siderite (Fig. 3a), in line with the high As removal efficiency. In contrast, the main XRD peaks of AAS-1.1 samples after reaction for 2–4 h were located at the same positions as those of standard XRD patterns of siderite (PDF #29-0696), thus indicating that the siderite was the dominant crystalline phase. After reaction for 10 h, the formation of scorodite was observed, and there was a substantial amount of siderite peaks remaining. This suggested that Na^+ and Cl^- ions were the critical factors for the dissolution of siderite and the crystallization of scorodite. After in AAS-0.4 system reaction for 2 h, the diffraction peaks of siderite were weaker than the AAS-1.1 system at the same reaction time, suggesting the fast dissolution rate of siderite. The XRD results showed that the scorodite became the dominant crystalline phase in the transformation products after the reaction for 4 h. This result suggests that the lower initial pH was the key factor for the dissolution–oxidation of siderite and the formation of scorodite.

The surface chemical properties of transformation products formed at different systems were investigated using FTIR spectroscopy (Fig. 3b). The v_1 stretching vibration band of As(V)-O located at ~822 cm^{-1} confirms the formation of the scorodite [34,41]. Correspondingly, the characteristic bands located at ~3,517 cm^{-1} are ascribed to the stretching vibration of H_2O/O–H from scorodite crystal [42]. The characteristic bands in the range of 900–1,200 cm^{-1}, are assigned to the stretching vibration of CO_3 in siderite [35]. The stretching vibration of siderite in the AAS-0.4 system was always weaker than the AAS-1.1 system at the same reaction time.

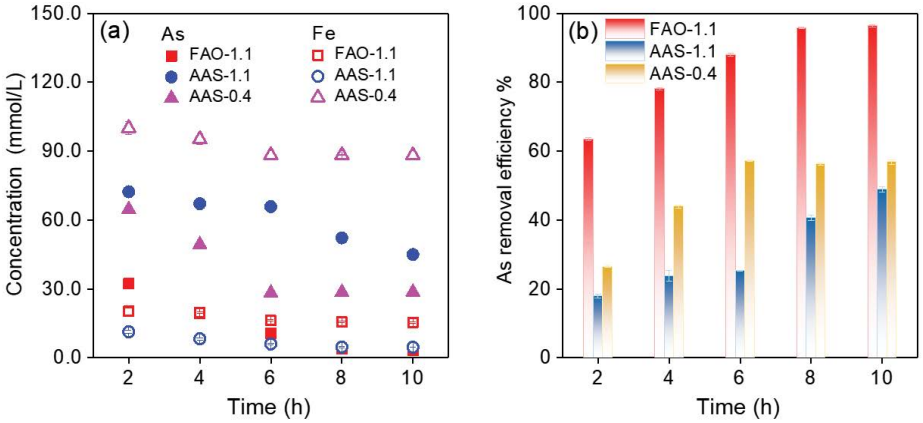

Fig. 2. Concentration of dissolved As and Fe (a) and the removal efficiency of As (b) as function of reaction times in the different systems.

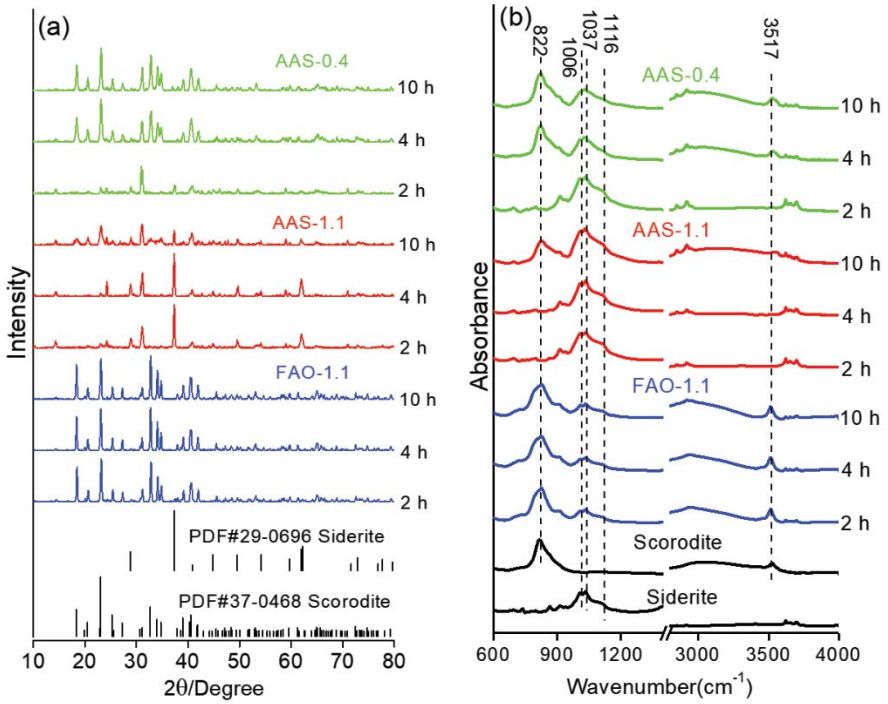

Fig. 3. X-ray diffraction patterns (a) and Fourier-transform infrared spectra (b) of standard materials and transformation solid products formed at different reaction time in various systems. The green, red, and blue lines represent the transformation products formed in AAS-0.04, AAS-1.1, and FAO-1.1, respectively.

These results suggest that lower initial pH is the key factor for facilitating the dissolution–oxidation of siderite and the formation of scorodite, which was in agreement with the XRD results.

The transformation products generated after 10 h at different systems are also characterized using scanning electron microscopy (Fig. 4). The results showed that the transformation products formed in the FAO-1.1 system appeared as rough surface spherical particles in the size of approximately 4–6 μm. This indicates that well-crystalline scorodite is formed. In contrast, the particles formed in the FAO-1.1 system appeared as irregularly shaped particles with a size of <2 μm. As the initial pH was reduced to 0.4 (AAS-0.4 system), the transformation products appeared as rough petal-shaped particles. Overall, lower initial pH can not improve As removal efficiency significantly, but it promotes siderite dissolution, providing a sufficient Fe source for scorodite formation and (Fe/As ratio of 3.1 in AAS-0.4) subsequent deep As removal.

3.3. Deep As removal via Fe-As coprecipitation

Lime neutralization and coprecipitation of Fe with As have been widely used for scavenging and fixation of As

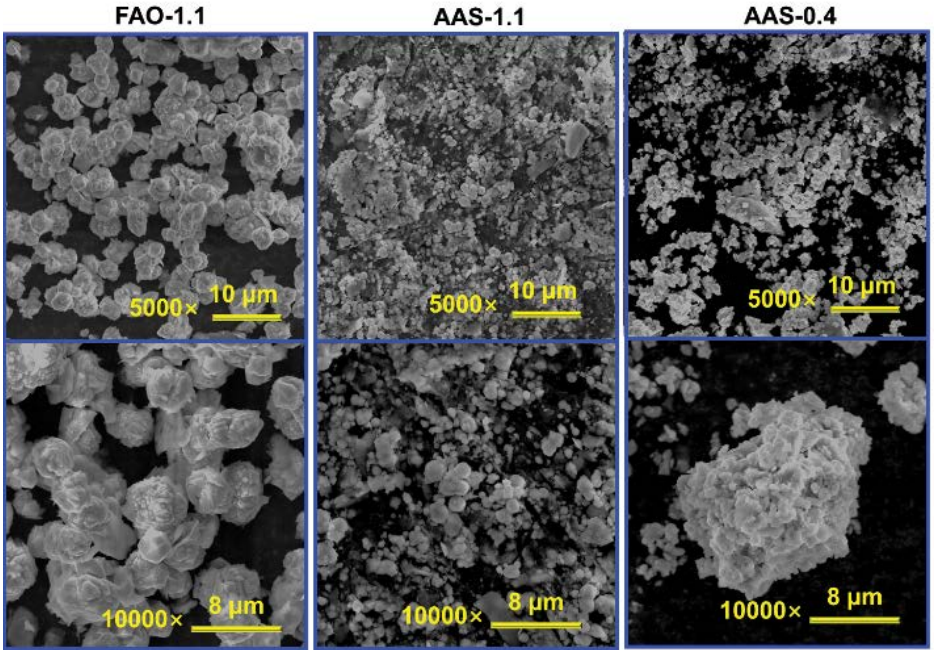

Fig. 4. Scanning electron microscopy images of transformation products in the different systems after reaction for 10 h.

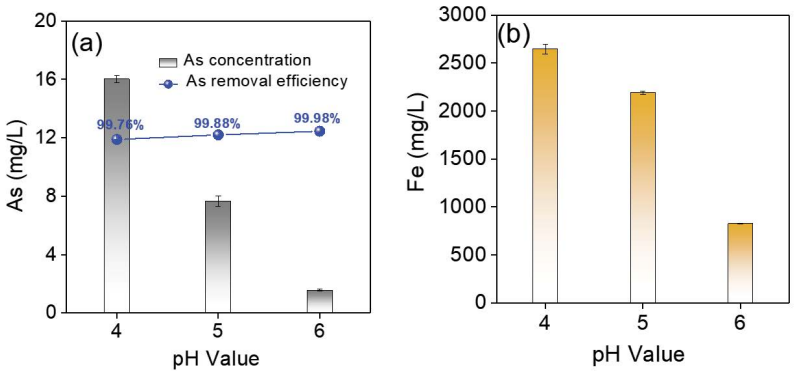

Fig. 5. Aqueous concentrations and removal efficiency of As (a), and concentrations of Fe (b) at different pH values.

from waste solution via the formation of ferric arsenate and arsenical ferrihydrite [43–46]. The removal of aqueous As is highly dependent on pH value. The optimal pH range for removing arsenate is 3.5–5.5, after which the concentration of arsenic in solution increases with increasing pH [47]. Fig. 5 shows the concentration of As and Fe in the AAS-0.4 system as a function of the pH value. The residual concentrations of aqueous As were 16.1, 7.62, and 1.57 mg/L at pH of 4, 5 and 6, corresponding to the removal efficiency of 99.76%, 99.88%, and 99.98%, respectively (Fig. 5a). The concentrations of residual Fe decreased from 2,646 to 827 mg/L with increasing pH value from 4 to 6 (Fig. 5b). This result suggests that a pH of 6 favors the As immobilization via Fe-As coprecipitation method.

3.4. Stability of the final products

The concentration of As in the TCLP test of final products was 251.8 mg/L, indicating that the solids were poorly crystalline phases, in agreement with solid phase characterization (Fig. 6a). In contrast, the concentration of As in the TCLP mixture of scorodite and Fe-As coprecipitation was satisfactory (2.6 mg/L), which was due to dissolution of poorly-produced scorodite could cause a significant release of As, however, the released As would be re-stabilized via re-adsorption or formation of Fe-As coprecipitation. This indicates that the Fe-As coprecipitate could enhance the stability of scorodite. The long-term stability of scorodite and scorodite and Fe-As coprecipitates mixture after 50 d was compared. For the scorodite, the final As concentration was 165.82, 193.81, and 204.47 mg/L at pH 4, 6, and 8, respectively, after 50 d, also implying that scorodite synthesized from this study had unsafe stability (Fig. 6b). In contrast, the long-term stability of scorodite and Fe-As coprecipitates mixture was satisfactory after 50 d, the final As concentration was 1.84, 2.13, and 3.20 mg/L with an increase of pH from 4 to 8 (Fig. 6c). Therefore, the final products can be safely stored in the environment.

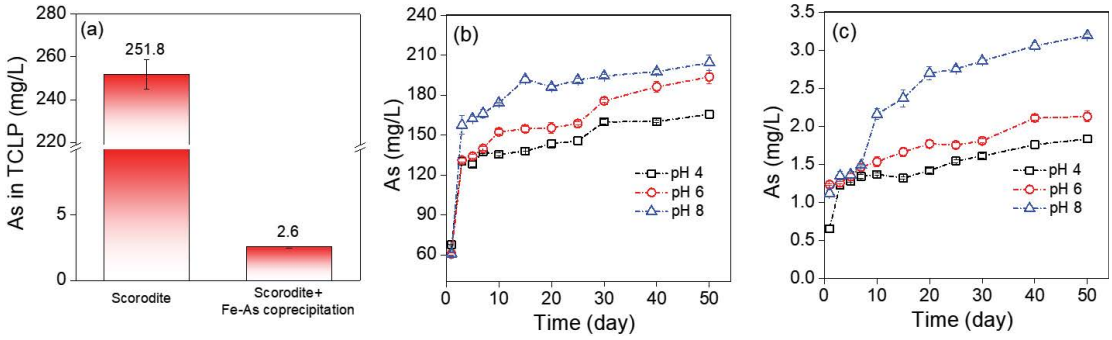

Fig. 6. The As in Toxicity Characteristic Leaching Procedure between scorodite and mixed of scorodite and Fe-As coprecipitation (a), long-term stability of scorodite (b), and mixed of scorodite and Fe-As coprecipitation (c).

3.5. Industrial application problem

The process flowsheet for the treatment of AAS is shown in Fig. 7. After the recovery of carbonate from the AAS leading liquor, hydrochloric acid is used for acidization to fix As via scorodite formation. Natural siderite is used as a Fe source in the formation of scorodite, with continuous air injection. Finally, deep As removal was conducted via the Fe-As coprecipitation method by neutralizing with slaked lime.

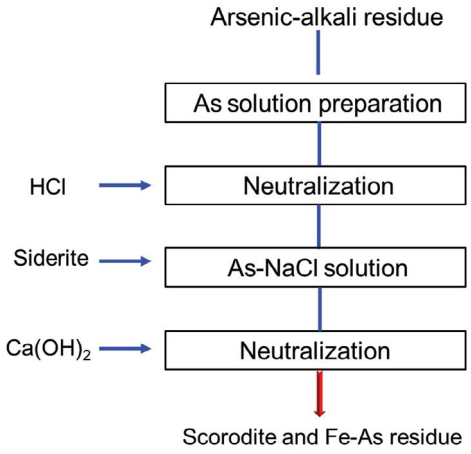

Fig. 7. Process flowsheet of arsenic-alkali slag treatment.

The research status of the AAS treatment method is presented in Table 3. The transformation of AAS to symplesite is difficult under anaerobic conditions, even though symplesite is a stable As-carrier. The cement solidification/stabilization treatment would significantly increase the bulk volume of the residue. Arsenic trioxide and arsenide sulfur easily release arsenic into the natural environment via the dissolution reaction. The Fe-As coprecipitation is an ideal method for AAS treatment because of the high stability of the Fe-As residue. However, the demand for the Fe source in this method is high. In addition, the cost of $Fe_2(SO_4)_3{\cdot}9H_2O$ reagent is also expensive. The fatal defect of the crystallization method is that the final product is usually not a single

Table 4
Economic evaluation of industrial-scale treatment for per ton arsenic-alkali slag. (The unit price of chemical reagents is from Chinese Suppliers)

Process chemical reagents	Price (USD/ton)	Doses (kg/ton)	Cost (USD/ton)
Neutralization 31% HCl	69	273	18.8
Precipitation–crystallization $FeCO_3$	119	145	17.3
Neutralization–precipitation CaO	102	45	4.6
Total	–	–	40.7

Table 3
Research status of the arsenic-alkali slag treatment

Reagent	As-carrier	Study
$FeSO_4{\cdot}7H_2O$	Symplesite	Wang et al. [9]
Combined Fe salts	Ferric arsenate	Han et al. [10]
Cement material	As-cement	Jiang et al. [11]
SO_2 gas	Arsenic trioxide	Long et al. [7]; Long et al. [12]; Long et al. [13]
Na_2S	Arsenide sulfur	Qiu et al. [48]; Wei and Deng [49]
$Fe_2(SO_4)_3{\cdot}9H_2O$	Fe-As residue	Su et al. [6]; Xiang et al. [26]
—	Mixed sodium arsenic	Chen et al. [2]; Deng et al. [3]; Li et al. [50]
Mg salt	Magnesium arsenate	Tian et al. [5,37]
Siderite	Scorodite + Fe-As residue	This work

arsenic-bearing solid, but a new arsenic-containing residue, the mixed residue of sodium carbonate and sodium arsenic. In the application of AAS treatment, although the formation of (ammonium) magnesium arsenate in an alkaline solution, its stability is not as good as that of Fe-As residue, so it has not been widely used.

The reagent cost of our proposed method for AAS treatment was calculated, when HCl, $FeCO_3$, and CaO were used. The reagent cost was calculated according to 3.7 wt.% As in AAS, the concentration of $NaHCO_3$ was 96 g/L when carbonate was recovered, and the pH increased from 0.4 to 6.0. The evaluated reagent cost is nearly 90.7 USD/ton AAS (Table 4), which is significantly lower than that of previous technologies, as siderite is a cost-effective Fe source.

4. Conclusions

In this study, an alternative treatment method for scavenging and fixation of metallurgical arsenic-alkali slag is proposed. The major contributions of this work include: (1) providing an alternative treatment method for arsenic removal and fixation in metallurgical arsenic-alkali slag at a suitable cost (40.7 USD/ton), (2) immobilizing As from AAS via scorodite and Fe(III)-As(V) coprecipitation, the final removal efficiency of As reaches 99.98%. (3) The mixture of scorodite and Fe-As coprecipitation showed good long-term stability at pH 4 6 and 8.

Author contributions statement

Xinrong Su: Experiments, writing manuscript and editing. Rui Su: Data interpretation, chemical analysis and editing. Yanjiao Gao: Chemical analysis, editing. Yinwen Bai: Experiments. Xuanyu Li: Experiments. Baochuan Qi: Conceptualization, data interpretation, editing and writing.

Declaration of interests

The authors declare that they have no known competing financial interests or personal relationships that could have appeared to influence the work reported in this paper.

Acknowledgments

We thank the Liaoning Provincial Natural Science Foundation Program Project (No. 2022-BS-312), Liaoning University of Technology Doctoral Research Start-up Fund Project (No. XB2021013), the Yili Normal University General Projects (No. 2023YSYB012).

References

[1] K. Wang, Q. Wang, Y. Chen, D. Li, Q. Tian, X. Guo, Status of solid waste disposal in antimony metallurgy, Nonferrous Met. Sci. Eng., 13 (2022) 8–17.
[2] B. Chen, Z. Wang, Z. Zhou, G. Hu, Y. Qiu, Commercial test of cleanly production technology of second arsenic-alkali residue, Min. Metall. Eng., 27 (2007) 47–49.
[3] W. Deng, L. Chai, Y. Dai, Industrial experimental study on comprehensive recoverying valuable resources from antimony smelting arsenic-alkali residue, Hunan Nonferrous Met., 30 (2014) 24–27.
[4] J. Li, H. Liang, Treatment strategies study on the comprehensive utilization of arsenic-alkali residue in Xikuangshan area, Hunan Nonferrous Met., 26 (2010) 53–55.
[5] J. Tian, Y. Wang, X. Zhang, W. Sun, H. Han, Z. Yu, T. Yue, A novel scheme for safe disposal and resource utilization of arsenic-alkali slag, Process Saf. Environ. Prot., 156 (2021a) 429–437.
[6] R. Su, X. Ma, J. Lin, E. Heredia, R. Chernikov, S. Wang, Y. Jia, An alternative method for the treatment of metallurgical arsenic-alkali residue and recovery of high-purity sodium bicarbonate, Hydrometallurgy, 202 (2021) 105590, doi: 10.1016/j.hydromet.2021.105590.
[7] H. Long, Y. Zheng, Y. Peng, H. He, Recovery of alkali, selenium and arsenic from antimony smelting arsenic-alkali residue, J. Cleaner Prod., 251 (2019) 119673, doi: 10.1016/j.jclepro.2019.119673.
[8] X. Guo, K. Wang, M. He, Z. Liu, H. Yang, S. Li, Antimony smelting process generating solid wastes and dust: characterization and leaching behaviors, J. Environ. Sci., 26 (2014) 1549–1556.
[9] X. Wang, J. Ding, L. Wang, S. Zhang, H. Hou, J. Zhang, J. Chen, M. Ma, C. Daniel, X. Wu, Stabilization treatment of arsenic-alkali residue (AAR): effect of the coexisting soluble carbonate on arsenic stabilization, Environ. Int., 135 (2020) 105406, doi: 10.1016/j.envint.2019.105406.
[10] F. Han, L. Shao, X. Shi, X. Liu, C. Li, Study on stabilizing and curing agent and method for arsenic residue, Hunan Nonferrous Met., 33 (2017) 65–77.
[11] G. Jiang, X. Min, Y. Ke, Y. Liang, X. Yan, W. Xu, Z. Lin, Solidification/stabilization of highly toxic arsenic-alkali residue by MSWI fly ash-based cementitious material containing Friedel's salt: efficiency and mechanism, J. Hazard. Mater., 425 (2022) 127992, doi: 10.1016/j.jhazmat.2021.127992.
[12] H. Long, Y. Zheng, Y. Peng, G. Jin, W. Deng, S. Zhang, H. He, Separation and recovery of arsenic and alkali products during the treatment of antimony smelting residues, Miner. Eng., 153 (2020a) 106379, doi: 10.1016/j.mineng.2020.106379.
[13] H. Long, X. Huang, Y. Zheng, Y. Peng, H. He, Purification of crude As_2O_3 recovered from antimony smelting arsenic-alkali residue, Process Saf. Environ. Prot., 139 (2020b) 201–209.
[14] G. Zeng, H. Li, S. Chen, X. Tu, W. Wang, Leaching kinetics and separation of antimony and arsenic from arsenic alkali residue, Adv. Mater. Res., 402 (2011) 57–60.
[15] Y. Li, Z. Liu, Q. Li, F. Liu, Z. Liu, Alkaline oxidative pressure leaching of arsenic and antimony bearing dusts, Hydrometallurgy, 166 (2016) 41–47.
[16] J. Wang, Hydrometallurgical process for recovery of antimony from arsenic-alkali residue, Tech. Equip. Environ. Pollut. Control, 7 (2006) 64–67.
[17] Y. Qiu, B. Lu, B. Chen, Y. Zhong, F. Wei, Y. Yang, Commercial scale test of anti-pollution control technique for slag of arsenic and soda, J. Cent. South Univ. Technol., 36 (2005) 234–238.
[18] R. De Klerk, Y. Jia, R. Daenzer, M. Gomez, G. Demopoulos, Continuous circuit coprecipitation of arsenic(V) with ferric iron by lime neutralization: process parameter effects on arsenic removal and precipitate quality, Hydrometallurgy, 111–112 (2012) 65–72.
[19] Y. Jia, D. Zhang, R. Pan, L. Xu, G. Demopoulos, A novel two-step coprecipitation process using Fe(III) and Al(III) for the removal and immobilization of arsenate from acidic aqueous solution, Water Res., 46 (2012) 500–508.
[20] Y. Du, Q. Lu, H. Chen, Y. Du, D. Du, A novel strategy for arsenic removal from dirty acid wastewater via $CaCO_3$-$Ca(OH)_2$-Fe(III) processing, J. Water Process Eng., 12 (2016) 41–46.
[21] E. Balladares, O. Jerez, F. Parada, L. Baltierra, C. Hernández, E. Araneda, V. Parra, Neutralization and co-precipitation of heavy metals by lime addition to effluent from acid plant in a copper smelter, Miner. Eng., 122 (2018) 122–129.
[22] J. Lei, B. Peng, Y. Liang, X. Min, Y. Chai, Y. Ke, Y. You, Effects of anions on calcium arsenate crystalline structure and arsenic stability, Hydrometallurgy, 177 (2018) 123–131.
[23] E. Li, T. Yang, Q. Wang, Z. Yu, S. Tian, J. Wang, Long-term stability of arsenic calcium residue (ACR) treated with $FeSO_4$ and H_2SO_4: function of H^+ and Fe(II), J. Hazard. Mater., 420 (2021) 126549, doi: 10.1016/j.jhazmat.2021.126549.

[24] D. Zhang, S. Wang, Y. Wang, M. Gomez, Y. Jia, The long-term stability of calcium arsenates: implications for phase transformation and arsenic mobilization, J. Environ. Sci., 84 (2019) 29–41.
[25] A. Nazari, R. Radzinski, A. Ghahreman, Review of arsenic metallurgy: treatment of arsenical minerals and the immobilization of arsenic, Hydrometallurgy, 174 (2017) 258–281.
[26] X. Xiang, L. Chai, X. Min, Y. Zhang, R. Deng, W. Jiang, A study on the removal of arsenic from leaching liquor of arsenic-containing alkaline dregs by precipitation as ferric arsenates, China Manganese Ind., 24 (2006) 30–33.
[27] B. Das, Theoretical study of formation of secondary arsenic minerals: scorodite and pharmacosiderite, ACS Earth Space Chem., 3 (2019) 192–201.
[28] X. Ma, Z. Yuan, G. Zhang, J. Zhang, X. Wang, S. Wang, Y. Jia, Alternative method for the treatment of hydrometallurgical arsenic–calcium residues: the immobilization of arsenic as scorodite, ACS Omega, 5 (2020) 12979–12988.
[29] X. Ma, M. Gomez, Z. Yuan, G. Zhang, Wang, S. Li, S. Yao, X. Wang, Y. Jia, A novel method for preparing an As(V) solution for scorodite synthesis from an arsenic sulphide residue in a Pb refinery, Hydrometallurgy, 183 (2019) 1–8.
[30] Y. Sun, Q. Yao, X. Zhang, H. Yang, N. Li, Z. Zhang, Z. Hao, Insight into mineralizer modified and tailored scorodite crystal characteristics and leachability for arsenic-rich smelter wastewater stabilization, RSC Adv., 8 (2018) 19560–19569.
[31] X.J. Qi, Y.K. Li, L.H. Wei, F.Y. Hao, X. Zhu, Y.G. Wei, K.Z. Li, H. Wang, Disposal of high-arsenic waste acid by the stepwise formation of gypsum and scorodite, RSC Adv., 10 (2020) 29–42.
[32] Y. Li, X. Zhu, X. Qi, B. Shu, X. Zhang, K. Li, Y. Wei, F. Hao, H. Wang, Efficient removal of arsenic from copper smelting wastewater in form of scorodite using copper slag, J. Cleaner Prod., 270 (2020) 122428, doi: 10.1016/j.jclepro.2020.122428.
[33] X. Li, G. Cai, Y. Li, X. Zhu, X. Qi, X. Zhang, B. Shu, K. Li, Y. Wei, H. Wang, Limonite as a source of solid iron in the crystallization of scorodite aiming at arsenic removal from smelting wastewater, J. Cleaner Prod., 278 (2021) 123552, doi: 10.1016/j.jclepro.2020.123552.
[34] G. Cai, X. Zhu, K. Li, X. Qi, Y. Wei, H. Wang, F. Hao, Self-enhanced and efficient removal of arsenic from waste acid using magnetite as an *in-situ* iron donator, Water Res., 157 (2019) 269–280.
[35] R. Su, X. Ma, X. Yin, X. Zhao, Z. Yan, J. Lin, X. Zeng, D. Zhang, S. Wang, Y. Jia, Arsenic removal from hydrometallurgical waste sulfuric acid via scorodite formation using siderite ($FeCO_3$), Chem. Eng. J., 424 (2021) 130552, doi: 10.1016/j.cej.2021.130552.
[36] X. Ma, R. Su, X.Y. Zhu, Z.X. Zhao, X.F. Zeng, S.F. Wang, Y.F. Jia, An innovative strategy for efficient and economical arsenic removal in hydrometallurgical waste sulfuric acid by co-treatment with Fe-As coprecipitation residue via scorodite formation, J. Cleaner Prod, 375 (2022) 134186, doi: 10.1016/j.jclepro.2022.134186.
[37] J. Tian, W. Sun, X. Zhang, H. Han, Z. Yu, T. Yue, L. Wang, Y. Yang, H. Tang, E. Li, Comprehensive utilization and safe disposal of hazardous arsenic-alkali slag by the combination of beneficiation and metallurgy, J. Cleaner Prod., 295 (2021b) 126381, doi: 10.1016/j.jclepro.2021.126381.
[38] R. Su, B. Qi, L. Zhao, Y. Gao, Study on the effect of ionic strength on the crystallization process of scorodite and fixation of arsenic, Appl. Chem. Ind., 51 (2022) 3207–3211.
[39] C. Silva, X. Liu, F. Millero, Solubility of siderite ($FeCO_3$) in NaCl solutions, J. Solution Chem., 31 (2002) 97–108.
[40] H. Itou, Mechanism of Scorodite Formation at Ambient Temperature as Determined by TEM Analysis, Paper Presented at: International Symposium on Iron Control Technologies, 2006.
[41] Y. Jia, L. Xu, X. Wang, G. Demopoulos, Infrared spectroscopic and X-ray diffraction characterization of the nature of adsorbed arsenate on ferrihydrite, Geochim. Cosmochim. Acta, 71 (2007) 1643–1654.
[42] X. Ma, S. Li, Z. Yuan, S. Yao, Y. Jia, S. Wang, Stabilization of scorodite by aluminum silicate microencapsulation, J. Environ. Eng., 145 (2019) 04019010, doi: 10.1061/(ASCE)EE.1943-7870.0001511.
[43] G. Waychunas, B. Rea, C. Fuller, J. Davis, Surface chemistry of ferrihydrite: part 1. EXAFS studies of the geometry of coprecipitated and adsorbed arsenate, Geochim. Cosmochim. Acta, 57 (1993) 2251–2269.
[44] W. Richmond, M. Loan, J. Morton, J. Parkinson, Arsenic removal from aqueous solution via ferrihydrite crystallization control, Environ. Sci. Technol., 38 (2004) 2368–2372.
[45] B. Moldovan, M. Hendry, Characterizing and quantifying controls on arsenic solubility over a pH range of 1–11 in a uranium mill-scale experiment, Environ. Sci. Technol., 39 (2005) 4913–4920.
[46] Y. Jia, G. Demopoulos, Coprecipitation of arsenate with iron(III) in aqueous sulfate media: effect of time, lime as base and co-ions on arsenic retention, Water Res., 42 (2008) 661–668.
[47] E. Krause, V.A. Ettel, Solubilities and stabilities of ferric arsenate compounds, Hydrometallurgy, 22 (1989) 311–337.
[48] Y.H. Qiu, B.Q. Lu, B.Z. Chen, Y. Zhong, W. Fu, Y.Q. Yang, Commercial-scale test of anti-pollution control technique for slag of arsenic and soda, J. Cent. South Univ. Technol., 36 (2005) 234–237.
[49] Y.S. Wei, X.W. Deng, Arsenic removal kinetics of hydrothermal sulfide precipitation for arsenic-alkali residue from antimony smelting, Nonferrous Met. (Smelting Part), 1 (2014) 8–11.
[50] Z. Li, W. Chen, C. Jin, The process research for separation of arsenic-alkali residue by fractional crystallization, Hunan Nonferrous Met., 31 (2015) 23–28.

Supplementary information

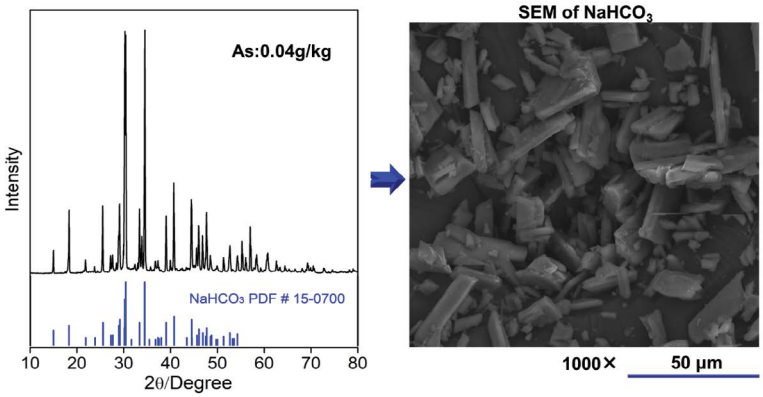

Fig. S1. X-ray diffraction patterns and SEM-EDX images of $NaHCO_3$. The vertical bars represent the standard X-ray diffraction patterns of $NaHCO_3$ (PDF#15-0700).